2D carbon sheets with negative Gaussian curvature assembled from pentagonal carbon nanoflakes

Cunzhi Zhang,[1] Fancy Qian Wang,[2] Jiabing Yu,[1] Sheng Gong,[1] Xiaoyin Li,[2] and Qiang Sun[1,2,*]

[1]Department of Materials Science and Engineering, College of Engineering, Peking University, Beijing 100871, China

[2]Center for Applied Physics and Technology, Peking University, Beijing 100871, China

Buckled Cario pattern

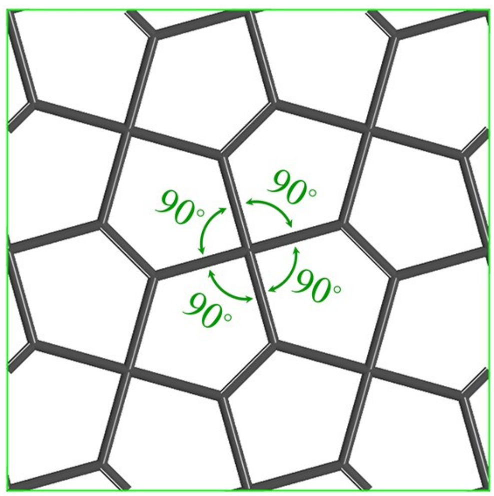

Fig. S1 Flat Cario pattern.

In Fig. S1, we show the 2D flat Cario pattern, within it the four-fold symmetry requires all pentagons must have 90° inner angles. When we have inner angle, α, larger than 90°, then the 2D space is not sufficient to accommodate these pentagons with 4α> 360° when put them together. As a result, a buckled 2D pattern is expected, and this is the reason why our CG_{568} allotropes are highly curved.

Phonon spectra from empirical potential

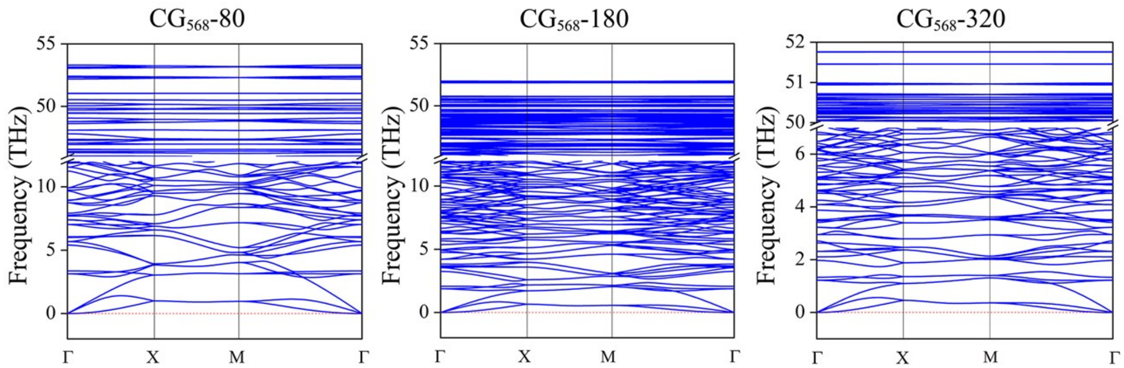

Fig. S2 Phonon spectra of CG_{568}-80, CG_{568}-180 and CG_{568}-320 calculated from Tersoff empirical potential.

To obtain phonon spectra, we need to first calculate harmonic interatomic force constants (IFCs). In our case, the structures are pretty large with hundreds of atoms per unit cell. Hence, we choose to calculate IFCs based on Tersoff empirical potential as complements to first principle results in Fig. 3b. Since all carbon atoms in CG_{568} structures share similar bonding features as graphene, with slight deviation from perfect sp^2 hybridization, we believe Tersoff potential, which is optimized to better reproduce the acoustic phonon frequencies and group velocities of graphene, could properly describe the bonding in our structures. Then the harmonic IFCs are calculated by finite displacement method in conjunction to LAMMPS package, and the phonon spectra are calculated by diagonalizing the dynamical matrix constructed from IFCs obtained. The results for three new carbon allotropes are presented in Fig. S2. It is clear that no imaginary phonon modes are observed for all three structures in the entire Brillouin zone.

Tiny dip of acoustic phonon branch near Γ

According to classical mechanics, a 2D material would have one particular transverse acoustic branch with quadratic dispersion near the Γ point, which is pretty sensitive to numerical accuracy. Even for some stable 2D materials, acoustic modes with negative frequencies of small magnitude can appear due to numerical inaccuracies. Especially in our case, where cell size is pretty large and Brillouin zone is rather small, those phonon modes of tiny negative frequencies in Fig. 3 are actually of very small wave vector k (very long wave length). In fact, such tiny dip of acoustic phonon branch near Γ has been observed in other systems.[1-5]

Molecular Dynamics simulations

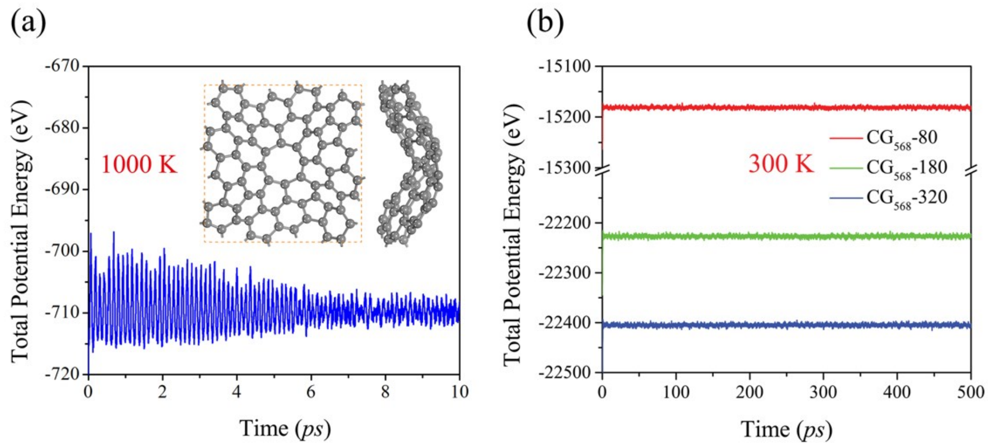

Fig. S3 Fluctuation of potential energy. (a) NVT FPMD simulation (1×1×1 unitcell), the inset is snapshot of structure at the end of simulation. (b) NVT MD based on Tersoff empirical potential (CG_{568}-80:5×5×1 supercell; CG_{568}-180: 4×4×1 supercell; CG_{568}-320:3×3×1 supercell).

To understand the dynamical stability of our new carbon sheets, we carried out molecular dynamics (MD) simulations. In Fig. S3(a), we plot the fluctuation of potential energy of CG_{568}-80 during FPMD simulations using VASP at alleviated temperature (1000 K) up to 10 *ps*. Clearly, the structure maintains its stability at the end of simulation.

Due to high computational cost, we can afford only the FPMD simulation of CG_{568}-80 using its unit cell (~ 10 *ps*). Therefore, we launched MD calculations based on Tersoff empirical potential using LAMMPS with thousands of atoms as complements. In Fig. S3(b), we can see only random fluctuations of total potential energy around constant values demonstrating the stability of three structures at least at the empirical potential level.

Bond-length/angle and bond-length/angle variation distribution

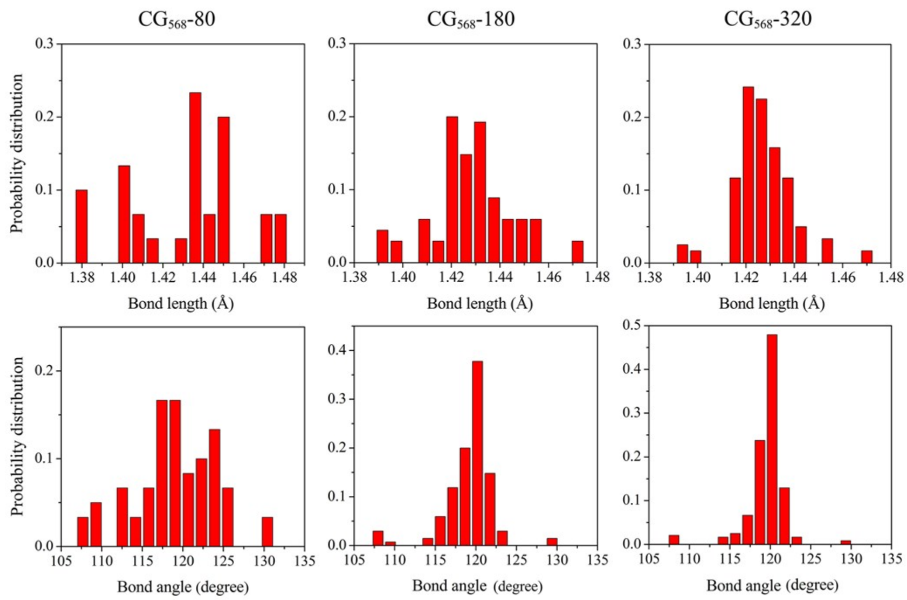

Fig. S4 C-C bond-length ∠CCC bond-angle distribution in three allotropes.

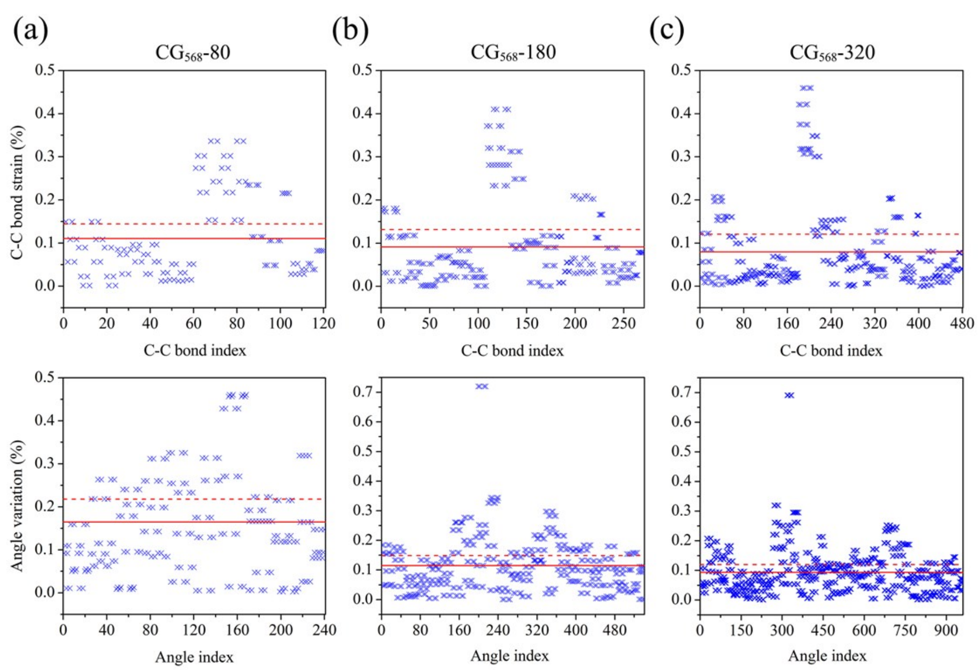

Fig. S5 Bond-length and bond-angle variation distribution (each bond and angle is given an index number). Red line: magnitude of $\overline{\varepsilon}$ and $\overline{\sigma}$; Red dash line: magnitude of $\overline{\varepsilon^2}$ and $\overline{\sigma^2}$. $\overline{\varepsilon} = \frac{1}{N}\sum_i^N |\varepsilon_i|$, $\overline{\varepsilon^2} = \frac{1}{N}\sum_i^N \varepsilon_i^2$, ε_i : i-th bond-length variation; $\overline{\sigma} = \frac{1}{N}\sum_i^N |\sigma_i|$, $\overline{\sigma^2} = \frac{1}{N}\sum_i^N \sigma_i^2$ σ_i : i-th bond-angle variation, N is the total number of bonds or angles.

Effective Mass

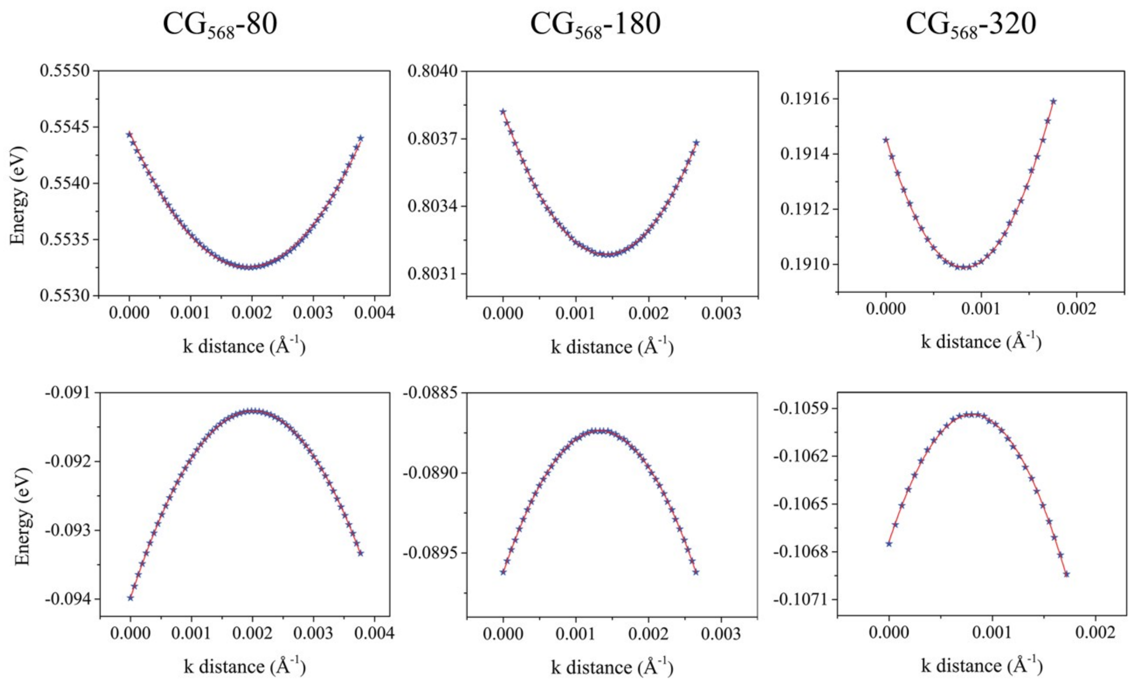

Fig. S6 Parabolic fitting of VBM and CBM (obtained from calculations using PBE). "k distance" is the distance between current k point and the first k point used for fitting.

Table S1 The locations of CBM and VBM in k-space.

Allotropes	VBM	CBM
CG_{568}-80	(0.396, 0.0)	(0.208, 0.208)
CG_{568}-180	(0.0, 0.0)	(0.176, 0.176)
CG_{568}-320	(0.461, 0.0)	(0.346, 0.346)

Deformation potential constants

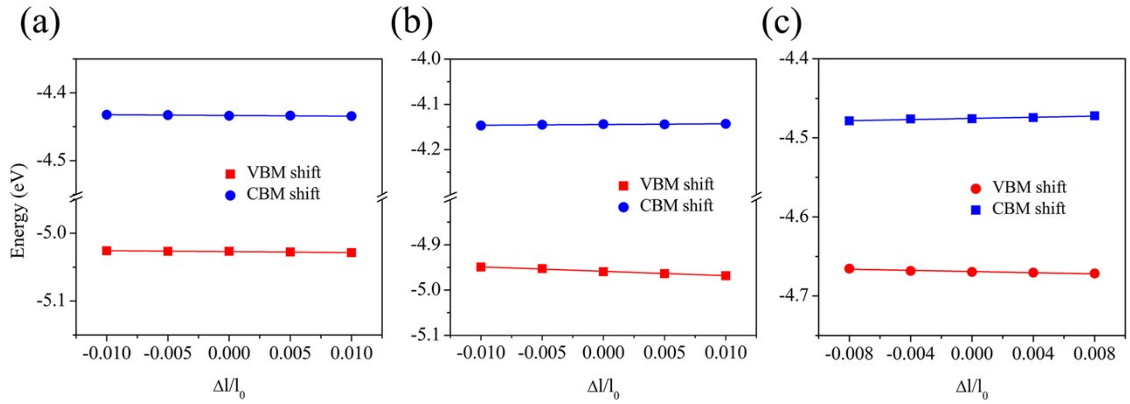

Fig. S7 Band edge position shifts of VBM and CBM of under lattice dilation or compression of CG_{568}-80 (a), CG_{568}-180 (b) and CG_{568}-320 (c). Δl refers to variation of lattice size, whereas l_0 refers to equilibrium lattice constant.

References

(1) Mannix, A. J.; Zhou, X. F.; Kiraly, B.; Wood, J. D.; Alducin, D.; Myers, B. D.; Liu, X.; Fisher, B. L.; Santiago, U.; Guest, J. R.; Yacaman, M. J.; Ponce, A.; Oganov, A. R.; Hersam, M. C.; Guisinger, N. P. *Science* **2015,** 350, 1513.
(2) Zhang, H.; Li, Y.; Hou, J.; Du, A.; Chen, Z. *Nano Lett.* **2016,** 16, 6124.
(3) Zhang, Z.; Liu, X.; Yakobson, B. I.; Guo, W. *J. Am. Chem. Soc.* **2012,** 134, 19326.
(4) Cahangirov, S.; Topsakal, M.; Aktürk, E.; Şahin, H.; Ciraci, S. *Phys. Rev. Lett.* **2009,** 102, 236804.
(5) Zhang, C.; Liu, J.; Shen, H.; Li, X.-Z.; Sun, Q. *Chem. Mater.* **2017,** 29, 8588.